

Radiosynthesis, *In Vitro* and *In Vivo* Evaluation of [¹⁸F]CBD-2115 as a First-in-Class Radiotracer for Imaging 4R-Tauopathies

Anton Lindberg, Ashley C. Knight, Daniel Sohn, Laszlo Rakos, Junchao Tong, April Radelet, N. Scott Mason, Jeffrey S. Stehouwer, Brian J. Lopresti, William E. Klunk, Johan Sandell, Alexander Sandberg, Per Hammarström, Samuel Svensson,* Chester A. Mathis,* and Neil Vasdev*

Cite This: *ACS Chem. Neurosci.* 2021, 12, 596–602

Read Online

ACCESS |

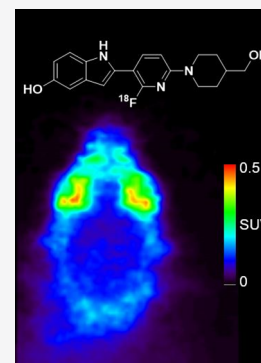
Metrics & More

Article Recommendations

Supporting Information

ABSTRACT: CBD-2115 was selected from a library of 148 compounds based on a pyridinyl-indole scaffold as a first-in-class 4R-tau radiotracer. *In vitro* binding assays showed [³H]CBD-2115 had a K_D value of 6.9 nM and a nominal B_{max} of 500 nM in 4R-tau expressing P301L transgenic mouse tissue. In binding assays with human brain tissue homogenates, [³H]CBD-2115 has a higher affinity (4.9 nM) for progressive supranuclear palsy specific 4R-tau deposits than [³H]flortaucipir (45 nM) or [³H]MK-6240 (>50 nM). [¹⁸F]CBD-2115 was reliably synthesized (3–11% radiochemical yield with molar activity of 27–111 GBq/ μ mol and >97% radiochemical purity). Dynamic PET imaging was conducted in mice, rats, and nonhuman primates, and all species showed initial brain uptake of 0.5–0.65 standardized uptake value with fast clearance from normal tissues. [³H]CBD-2115 could be a useful lead radioligand for further research in 4R-tauopathies, and PET radiotracer development will focus on improving brain uptake and binding affinity.

KEYWORDS: PET, tau, 4R-tau, fluorine-18, CBD-2115



Human tau exists in six isoforms varying in size from 352 to 441 amino acids that are distinguished by the number of inserts at the N-terminus (0N, 1N, or 2N) as well as the number of repeated microtubule binding domains (3R or 4R) at the C-terminus.¹ Tau is naturally without any specific secondary or tertiary structures, but it can take on multiple folded conformations after hyperphosphorylation.² Hyperphosphorylation and truncation of the native tau protein are important steps in early tauopathy.³

Development of biomarkers to assess the accumulation of tau protein in the living human brain is crucial to better understand the pathophysiology of non-Alzheimer's Disease (non-AD) tauopathies such as chronic traumatic encephalopathy (CTE),⁴ Pick's disease (PiD),⁵ progressive supranuclear palsy (PSP),⁶ and corticobasal degeneration (CBD).⁷ Such biomarkers will aid definitive diagnosis and confirm target engagement as well as dosing regimens of new therapies. While tau aggregation in PiD is considered to be primarily composed of 3R-tau, PSP and CBD aggregates are primarily 4R-tau, and AD and CTE aggregates are composed of a mixture of both 3R- and 4R-tau.

Major progress has been made toward development of positron emission tomography (PET) biomarkers for AD. While [¹¹C]PiB and the three U.S. Food and Drug Administration approved amyloid- β plaque PET radiopharmaceuticals ([¹⁸F]Amyvid, [¹⁸F]Neuraceq, and [¹⁸F]Vizamyl) have become available over the past decade for widespread imaging of amyloid plaques in AD,^{9–12} first generation, and

second generation AD tau-PET tracers are still emerging (Figure 1).¹³

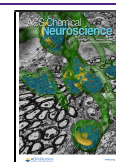
Development of 4R-tau selective PET imaging agents is among the biggest challenges in PSP and CBD research.^{14–16} These imaging agents are needed to guide multicenter trials (e.g., 4-Repeat Tauopathy Neuroimaging Initiative and Alzheimer's disease Neuroimaging Initiative) and patient selection for trials and drug development.^{17–20} Preliminary imaging studies have been carried out in PSP patients with [¹⁸F]PI-2620²¹ and [¹⁸F]PM-PBB3 (also known as APN-1607)²² (Figure 1).

A recent patent by CBD Solutions disclosed 148 compounds with the objective to develop a non-AD tau ligand based on a novel 2-(6-(piperidin-1-yl)pyridin-3-yl)-1H-indole structural scaffold (WO 2019/1917502 A1).²³ Compounds were designed according to established characteristics for a central nervous system (CNS) PET tracer²⁴ as well as affinity and selectivity toward 4R-tau. In the present study, the lead candidate, CBD-2115 (Figure 1F), was radiolabeled with ³H for *in vitro* evaluation in a transgenic mouse model (P301L) as

Received: December 18, 2020

Accepted: January 21, 2021

Published: January 26, 2021



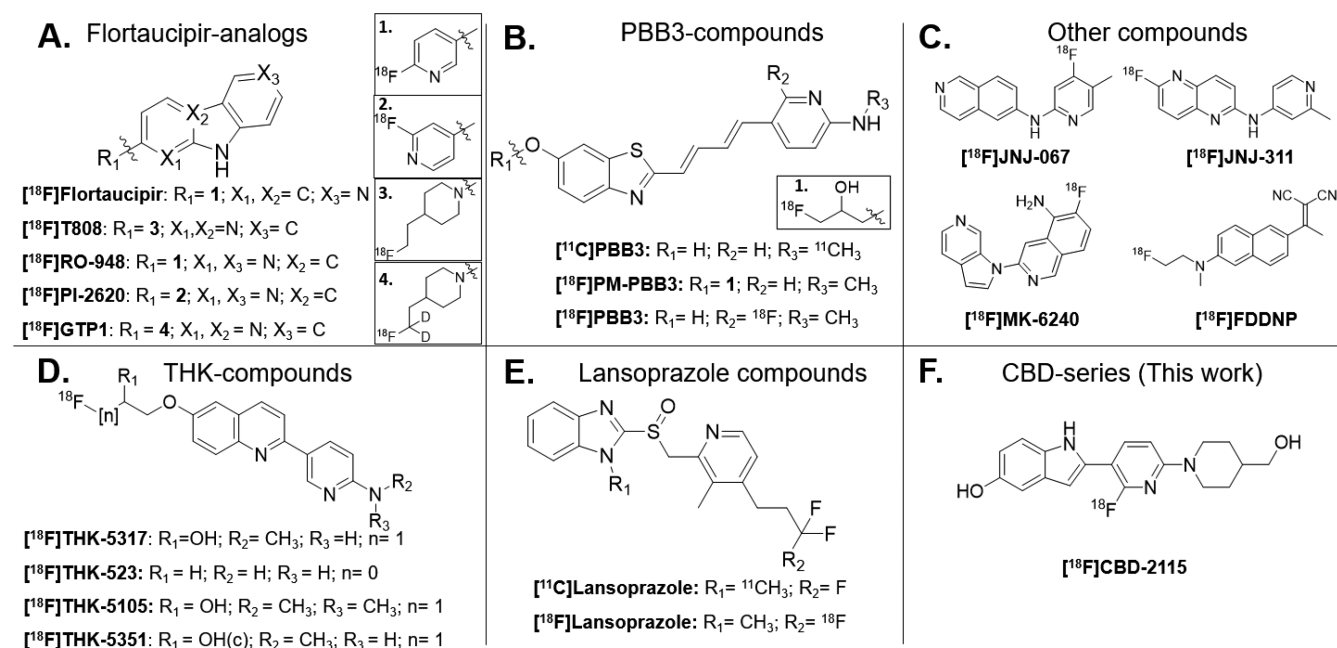


Figure 1. Tau PET radiotracers divided into structural scaffolds. (A) Compounds based on the carbazole scaffold of [¹⁸F]flortaucipir (also known as [¹⁸F]T807 or [¹⁸F]AV-1451). (B) PBB3 benzothiazole-butadienes. (C) Other compounds: Janssen's naphthalene-pyridine linked scaffolds, [¹⁸F]MK-6240 and [¹⁸F]FDDNP. (D) THK series of pyridinyl-quinoline ethers. (E) Lansoprazole isotopologues. (F) [¹⁸F]CBD-2115.

well as in human brain tissues (AD, PSP and CBD) for comparison with first and second generation radiotracers developed for tau-PET imaging in AD: [¹⁸F]flortaucipir and [¹⁸F]MK-6240, respectively (Figure 1 and Table 1). [¹⁸F]CBD-2115 was synthesized and evaluated *in vivo* with PET imaging in rodents (mouse and rat) and nonhuman primates.

Table 1. Comparison of Tau Radiotracers in Postmortem Tissues

sample tissue	[³ H]MK-6240	[³ H]flortaucipir	[³ H]CBD-2115
AD K _D (nM)	0.57 ± 0.33	1.9 ± 0.5	5.5 ± 1.9
PSP K _D (nM)	>50	45 ± 4	4.9 ± 0.2
CBD K _D (nM)	>50	33 ± 2	27 ± 1

RESULTS AND DISCUSSION

Pharmacological properties of CBD-2115 were promising for a CNS PET tracer. The *in vivo* stability of CBD-2115 was evaluated in liver microsomes of human (8.56 mL/min/kg) and rat (63.84 mL/min/kg). The efflux ratio measured in MDR1-MDCK cells determined that P-glycoprotein does not actively transport CBD-2115 (B-A/A-B ratios of 0.98 (Table S2). Free fraction in blood plasma was measured in both human (2.70%) and rat (2.85%). The CNS multiparameter optimization (MPO) desirability score²⁵ was calculated as 4.63. Scores over 4.0 (maximum 6.0) are considered good candidates for CNS drugs. CBD-2115 was screened for off-target selectivity (Eurofins, Kalamazoo, MI) toward 93 CNS receptors and enzymes, including MAO-A and MAO-B, with corresponding specific radioligands at a concentration of 1.0 μM. Results showed specific interaction of CBD-2115 with one target, the melatonin binding site (MT3(ML2)) on quinone dehydrogenase 2 (Table S1). Binding to MT3(ML2) is common among tau ligands, but expression in brain for

MT3(ML2) does not overlap with regions of interest (ROI) for non-AD tauopathies.

³H-labeled CBD-2115 was used in autoradiography experiments with cortical tissue from CBD and PSP patients, and the tau specific antibody AT-8 confirmed the presence of tau filaments in the postmortem tissue.²⁶

Through *in vitro* binding analyses, [³H]CBD-2115 was compared to tau PET tracers optimized for AD, [³H]MK-6240 and [³H]flortaucipir, in postmortem tissue homogenates from brains with neuropathologically confirmed diagnoses of AD, PSP, and CBD. As anticipated, [³H]MK-6240 followed by [³H]flortaucipir were more potent than [³H]CBD-2115 in AD tissue (Table 1). Promising data were revealed with [³H]CBD-2115 as the most potent radiotracer for 4R-tauopathies in CBD (K_D 27 ± 1 nM) and PSP (K_D 4.9 ± 0.2 nM) tissues.

[³H]CBD-2115 was evaluated in P301L transgenic mice with histologically confirmed 4R-tau aggregate expression (Figure 2). The measured K_D value of 6.9 nM was consistent with the human PSP tissue data, and had a nominal B_{max} of 500 nM.

The results from Scatchard analysis of *in vitro* binding assays with [³H]CBD-2115 indicate that this compound shows similar affinity for tau aggregates in human AD and PSP cases. High [³H]CBD-2115 binding affinity was likewise observed in 4R-tau expressing P301L transgenic mouse brain tissues and this compound should prove to be a useful lead radioligand for further research in 4R-tauopathies.

RADIOCHEMISTRY

Protecting alcohols is a common strategy for radiofluorination as it reduces byproducts from reaction with [¹⁸F]fluoride. As CBD-2115 contains two such hydroxyl-groups, a two-step labeling sequence was initially explored with a precursor bearing methoxyethoxymethyl (MEM) protecting groups on both hydroxyl-groups and a *tert*-butyloxycarbonyl (BOC) protecting group on the indole nitrogen. This approach

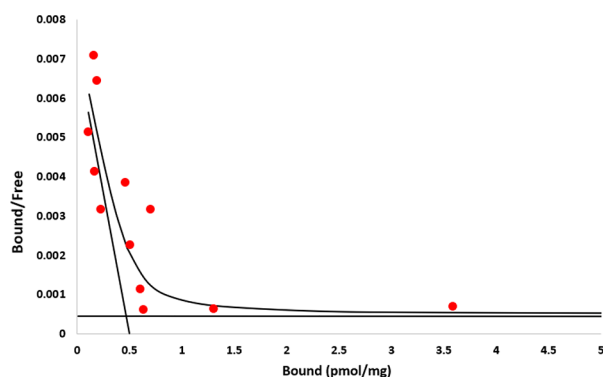


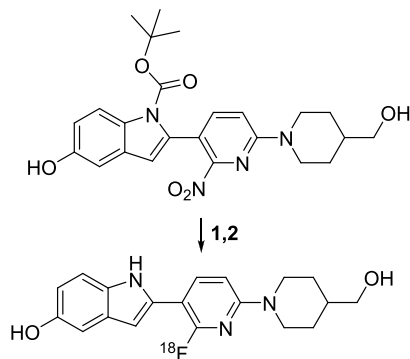
Figure 2. Scatchard plot of [^3H]CBD-2115 in P301L mouse tissue. [^3H]CBD-2115 has a measured K_D of 6.9 nM.

resulted in a 70% radiochemical conversion to the MEM and *N*-BOC-protected intermediate using K_2CO_3 and Kryptofix2.2.2 in DMSO at 160 °C. However, the resulting intermediate proved unstable to deprotecting conditions with acids, despite several attempts using trifluoroacetic acid, acetic acid, HCl, and the Lewis acid ZnCl_2 and varying temperatures between ambient and 150 °C. Alternative conditions tolerated by the molecule were too weak for removal of the MEM groups in our hands. Subsequent attempts to radiolabel a precursor with only the BOC protecting group on the indole nitrogen and unprotected hydroxyl-groups using identical radiofluorination conditions, followed by a removal of the BOC protecting group in methanol at 130 °C were successful. While this method significantly reduced the radiochemical conversion of the first step ($\sim 10\text{--}15\%$), the intermediate could be deprotected without degradation of the molecule to yield [^{18}F]CBD-2115, and formulated for *in vivo* studies. [^{18}F]CBD-2115 was reliably produced at two sites (Toronto and Pittsburgh) with high radiochemical purity (RCP) of 97–98% and was suitable for PET imaging studies in mice, rats, and nonhuman primates. The radiosyntheses yielded molar activity values (A_m) of 27.3 ± 6.2 GBq/ μmol and radiochemical yields (RCY) of $10.7 \pm 3.5\%$ ($n = 3$) (CAMH, Toronto), A_m of 111 GBq/ μmol ($n = 3$), and RCY of $2.8 \pm 1.5\%$ (University of Pittsburgh, PA) (Scheme 1).

PET IMAGING IN RODENTS

Dynamic PET imaging was performed in three wild-type (wt) male mice. Following bolus intravenous (i.v.) administration of

Scheme 1. Radiosynthesis of [^{18}F]CBD-2115^a



^aConditions: (1) [^{18}F]F $^-$, K_2CO_3 , Kryptofix2.2.2., DMSO, 140–160 °C, 20–30 min. (2) Methanol, 130 °C, 20 min.

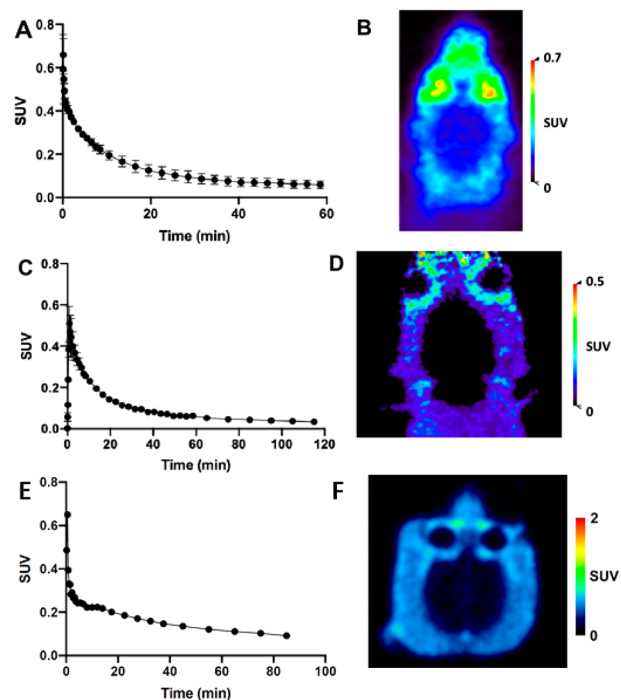


Figure 3. Time–activity curves (TACs) and PET summation images from PET measurements using [^{18}F]CBD-2115. (A) Whole brain TAC in mouse, (B) PET summation image (0–60 min) in mouse, (C) whole brain TAC in rat, (D) PET summation image (0–120 min) in rat, (E) whole brain TAC in NHP, and (F) PET summation image (0–90 min) in NHP.

[^{18}F]CBD-2115 (9.1 ± 1.1 MBq), radioactivity reached a maximum of 0.66 standardized uptake value (SUV) in whole brain and decreased to below 0.1 SUV after 30 min (Figure 3A and B). Although *in vitro* assays suggested that [^{18}F]CBD-2115 would be a useful PET radiotracer in mice, *in vivo* brain uptake is lower than what would be ideal for CNS applications (peak > 1 SUV). We further tested for a potential species difference in normal rats. Following i.v. administration of [^{18}F]CBD-2115 in two healthy rats (male and female, 15.5 and 16.5 MBq, respectively), radioactivity reached a maximum of 0.5 SUV in whole brain and decreased to below 0.1 SUV after 30 min (Figure 3C and D). Therefore, PET studies in rats and mice showed similar results with low initial brain uptake and moderate but steady washout. The lack of retention of radioactivity beyond 30 min was expected in healthy animals without specific 4R-tau inclusions in brain and suggest that there is little if any off-target binding *in vivo*. This is consistent with *in vitro* binding assays performed by Eurofins, in that CBD-2115 has no significant affinity for any of the 93 proteins evaluated including MAO-A and MAO-B, both of which have caused undesired off-target binding in some tau PET radiotracers.

PET IMAGING IN NONHUMAN PRIMATE (NHP)

To further explore this tracer in a higher species, one rhesus monkey was used in a baseline dynamic PET imaging study. Following i.v. administration of 185 MBq [^{18}F]CBD-2115, activity reached a peak of 0.65 SUV within the first 2 min and decreased to below 0.2 SUV after 25 min and remained below 0.2 SUV for the remainder of the 90 min scan (Figure 3E and F). Throughout the PET measurement, blood samples were collected for radiometabolite analysis. The fraction of

unmetabolized parent was 45% at 10 min and decreased below 20% after 30 min (Figure S1 and Table S3). The radiometabolite analysis revealed only one polar species that was rapidly formed and is unlikely to interfere with PET imaging of the CNS.

The results of PET measurements in NHP brain follows the results in rodents closely, and all species showed initially low brain uptake followed by rapid clearance. This likely precludes the use of [¹⁸F]CBD-2115 for further translation as an imaging agent for tau in human brain.

LIPOPHILICITY AND CNS MPO

The experimentally measured lipophilicity of [¹⁸F]CBD-2115, log_{D7.4} was determined to be 2.99 ± 0.15 in 1-octanol using the shake-flask method.²⁷ This value is lower than the calculated log_D value from ACD/I-lab of 3.45 and is within the range normally considered acceptable for a CNS PET radioligand.²⁴ Evaluating the low brain uptake of [¹⁸F]CBD-2115 in PET measurements using CNS MPO desirability scoring allowed for identifying potential issues that can be amended to improve brain uptake for future analogues from this new structural scaffold.²⁵ Using ACD/I-Lab predicted physiochemical properties along with the experimentally measured values of log_{D7.4} of CBD-2115 yielded a CNS MPO desirability score of 4.63.²⁵ While the overall score is comparable to many functional CNS PET radiotracers, a potential issue regarding hydrogen bond donors was identified, where CBD-2115 only scored 0.167 out of a possible 1.000, and this may offer a parameter for improvement.

[¹⁸F]CBD-2115 represents a new structural class of potential tau PET tracers with low off-target interaction exhibited in a broad CNS target screening assay. While binding selectivity for 4R-tau over 3R-tau and mixed 3R/4R-tau would be advantageous, a radioligand with high affinity to more than one type of tau aggregate would be useful in imaging more than one tauopathy type. The *K_D* of CBD-2115 for 4R-tau aggregates likely will need to be less than 1 nM to provide sufficient persistent imaging signal in non-AD tauopathy cases which typically have relatively low tau aggregate densities in the brain. Evaluation of [¹⁸F]CBD-2115 in rodents and NHP showed that brain uptake was less than desirable (2–5 SUV at early times) and will need to be increased. Further work is ongoing to develop new analogues of [¹⁸F]CBD-2115 with improved affinity to 4R-tau aggregates as well as higher brain uptake and will prioritize compounds with fewer hydrogen bond donors.

METHODS

Radiochemistry. [³H]CBD-2115. Calcium carbonate (2.6 mg, 26 μmol) was added to an ice slurry of NaBT₄ (1.7 mg, 45 μmol) in ethanol (300 μL) and tetrahydrofuran (THF; 300 μL). The mixture was stirred at 0 °C for 30 min. A solution of 1-(6-fluoro-5-(5-hydroxy-1H-indol-2-yl)pyridin-2-yl)piperidine-4-carbaldehyde (1.7 mg, 4.4 μmol) in THF (300 μL) was added, and the mixture was stirred for 2 h at 0 °C and then at ambient temperature for 2 h. Water was then added (500 μL), and the mixture was purified on reverse phase HPLC. The eluant was evaporated, and the residue was diluted in ethanol to afford 55 MBq of [³H]CBD-2115. MS *m/z* M + H (major peak) 342 (32%), 344 (48%), 346 (20%).

[¹⁸F]CBD-2115 (CAMH, Toronto). No-carrier-added [¹⁸F]F⁻ was produced via the ¹⁸O(p,n)¹⁸F reaction (Scanditronix MC-17 cyclotron) and transferred in [¹⁸O]water to a automated radio-synthesizer (GE Tracerlab FX2N) in a lead shielded hotcell. The [¹⁸F]F⁻ was trapped on a PS-HCO₃ ion exchange column (Chromafix) before being eluted with K₂CO₃ (1.37 mg, 10 μmol) and Kryptofix2.2.2 (14

mg, 5 μmol) in water/methanol (10/90, 1 mL) into the reaction vessel. Solvents were evaporated under vacuum and subsequently azeotropically dried with acetonitrile (1 mL) under continuous nitrogen flow. The precursor, *tert*-butyl 5-hydroxy-2-(6-(4-(hydroxymethyl)piperidin-1-yl)-2-nitropyridin-3-yl)-1H-indole-1-carboxylate (1.5 mg, 3.2 μmol), in DMSO (1 mL) was added, and the reactor was heated to 160 °C for 20 min. The reactor was cooled down to 70 °C, and methanol (1 mL) was added before heating to 130 °C for 20 min. The reactor was then cooled to 70 °C, and the reaction mixture was diluted with acetonitrile/water (20:80) before being injected onto a reverse phase HPLC column (Luna 10 μm C18(2) 100 Å, 250 mm × 10 mm, Phenomenex). The desired product was eluted with a mobile phase of acetonitrile-NH₄CO₂H_{aq} (0.05 M) (37/63, v/v) at a flow rate of 5 mL/min. The retention time of [¹⁸F]CBD-2115 was 10–13 min. The collected fraction was diluted with water (30 mL) and loaded onto a solid phase extraction (SPE) column (SepPak tC18, Waters). The SPE column was washed with water (10 mL) before [¹⁸F]CBD-2115 was eluted by ethanol (1 mL) and mixed with sterile saline (9 mL). The purity and *A_m* were determined by reverse-phase HPLC (Alltima C18, 4.6 × 250 mm, 5 μm, HiChrom), and the sample was eluted with acetonitrile–NH₄CO₂H (0.05 M) (40/60, v/v) at a flow rate of 3 mL/min (retention time = 5 min). Radiochemical identity was confirmed by coinjection of authentic standard with sample of final product formulation.

[¹⁸F]CBD-2115 (University of Pittsburgh). No-carrier-added [¹⁸F]F⁻ was produced via the ¹⁸O(p,n)¹⁸F reaction (Siemens Eclipse HP cyclotron) and transferred in [¹⁸O]water to a lead shielded hotcell. The [¹⁸F]F⁻ was trapped on QMA light SepPak (Waters) conditioned with 10 mL of 0.1 M aqueous sodium bicarbonate followed by 10 mL of Milli-Q water), before being eluted with K₂CO₃ (1.67 mg, 3.3 μmol) and Kryptofix2.2.2 (4.2 mg, 1.5 μmol) in acetonitrile/water (83:17, 1 mL) into the reaction vessel. Solvents were evaporated under argon flow at 110 °C. The residue was then azeotropically dried with acetonitrile (2 × 1 mL) to provide [¹⁸F]fluoride. The precursor, *tert*-butyl 5-hydroxy-2-(6-(4-(hydroxymethyl)piperidin-1-yl)-2-nitropyridin-3-yl)-1H-indole-1-carboxylate (5.0 mg, 10.6 μmol) in DMSO (1 mL) was added, and the reaction vessel was heated to 140 °C for 30 min. The reaction vessel was cooled down to 70 °C, and methanol (1 mL) was added before being heated to 130 °C for 20 min. The reaction vessel was then cooled to 70 °C, and the reaction mixture was diluted with water before being injected onto a reverse phase HPLC column (Luna 10 μm C18(2) 100 Å, 250 mm × 10 mm, Phenomenex). The desired product was eluted with a mobile phase of acetonitrile–NH₄CO₂H_{aq} (10 mM) (37/63, v/v) at a flow rate of 2 mL/min (0–5 min) and then 8 mL/min for the remainder of purification. The retention time of [¹⁸F]CBD-2115 was 10–13 min. The collected fraction was diluted with water (50 mL), and the solution was transferred across a SPE column (SepPak tC18, Waters). The SPE column was washed with water (10 mL) before [¹⁸F]CBD-2115 was eluted by ethanol (1 mL) and mixed with sterile saline (9 mL). The purity and *A_m* were determined by reverse-phase HPLC (4.6 × 250 mm, 5 μm, Luna C18(2), 5 μm) using a gradient (Solvent A: 10 mM ammonium formate; Solvent B: acetonitrile, 25–60% Solvent B over 20 min at a flow rate of 2 mL/min). Radiochemical identity was confirmed by coinjection of authentic standard with sample of final product formulation. The endotoxin level of the final formulation was <2.00 EU/mL (Charles Rivers Endosafe), and the administered mass was <1.0 μg in the nonhuman primate study.

Binding Studies with Brain Homogenates. Binding to brain homogenates for determination of *K_d* and *B_{max}* was performed with slight modifications of a procedure previously described in detail.²⁸ Briefly, frozen aliquots (–80 °C) of homogenized cortex (10 mg/mL in PBS) from AD, PSP, and CBD brains were thawed and diluted 10-fold in PBS (pH = 7.0) to 1 mg/mL. The unlabeled test compound (e.g., CBD-2115) was dissolved in DMSO at 400 μM and then diluted to 20 μM with PBS to yield 5% DMSO/PBS. The remaining serial dilutions (typically from 6 μM to 4 nM) were made with 5% DMSO/PBS to maintain a constant DMSO concentration in the final

assay. A volume of 50 μL of these solutions was combined with 50 μL of [^3H]CBD-2115 and 800 μL of PBS to yield 0.25% DMSO, ~ 1 nM tritiated compound, and 0.2–1000 nM unlabeled compound in the final assay. The assay began by addition of 100 μL of the 1 mg/mL brain homogenate to achieve a final concentration of 100 μg tissue/mL. After incubation for 60 min at room temperature, the binding mixture was filtered through a Whatman GF/B glass filter via a Brandel M-24R cell harvester (Gaithersburg, MD) and rapidly washed three times with 3 mL of PBS. The filters were counted in Cytoscint-ES after thorough vortexing and were stored overnight. All assays were performed at least in triplicate. The concentration of bound compound was determined from the radioactivity retained on the filter after correcting for the nondisplaceable radioactivity (defined as that remaining with ~ 1 μM unlabeled compound) and the specific activity of the tritiated compound after dilution with varying concentrations of unlabeled compound.

PET Imaging. Animal studies were carried out in accordance with the guidelines put forth by the institutional animal care and use committees at CAMH (mouse and rat studies) and the University of Pittsburgh (NHP study). Three healthy adult male mice (C57BL/6, 7.5-month old, 29–32 g) underwent 60 min dynamic PET imaging following bolus injection of [^{18}F]CBD-2115 (9.1 ± 1.1 MBq, $A_M = 18 \pm 10$ GBq/ μmol). Two healthy Sprague–Dawley rats (male, 358 g; and female, 241 g; 3 months old) underwent 120 min dynamic PET imaging following the injection of [^{18}F]CBD-2115 (15.5 and 16.5 MBq; $A_m = 19$ and 8 GBq/ μmol , respectively). PET images were acquired using a nanoScan PET/MRI (3T) scanner (Mediso, Budapest, Hungary). The acquired list-mode data were sorted into 33 frames (mice, 3×5 s, 3×15 s, 3×20 s, 7×60 s, and 17×180 s) or 39 frames (rats, 3×5 s, 3×15 s, 3×20 s, 7×60 s, 17×180 s, and 6×600 s) and binned into 3D true sinograms (ring difference: 84). The 3D sinograms were converted to 2D sinograms using Fourier-rebinning and reconstructed using a 2D-filtered back projection (FBKP) with a Hann filter at a cutoff of 0.50 cm^{-1} . A static image of the complete emission acquisition was reconstructed with the manufacturer's proprietary iterative 3D algorithm (6 subsets, 4 iterations). All image data were corrected for detector geometry and efficiencies, dead-time and decay corrected to the start of acquisition, without corrections for attenuation or scatter. Image analyses and extraction of brain TACs from the dynamic FBKP images were performed using VivoQuant (4.0 patch1, Invivo) with standard MR brain templates and atlases for rat and mice.^{29,30} SUV was calculated by normalizing regional radioactivity for injected radioactivity and body weight of the animal.

NHP (*Macaca mulatta*) imaging was performed on a Siemens Biograph mCT scanner. Prior to anesthetic induction, the monkey was sedated with ketamine (15 mg/kg, i.m.) and glycopyrrolate (0.01 mg/kg, i.m.) to control salivation and then intubated and administered isoflurane anesthesia (0.5–2.0% MAC) in a 40% mixture of oxygen/medical air. Vital signs, including pulse oximetry, blood pressure, respiratory rate, and end-tidal CO_2 , were monitored throughout the study. Two intravenous catheters were placed in right and left saphenous veins, one for radiopharmaceutical injection and fluid replacement and the second for blood sampling.

A low-dose CT scout scan was performed to facilitate positioning the animal such that the brain was in the central ~ 10 cm of the axial and transaxial scanner field-of-view where peak sensitivity and resolution are realized. Once positioned, a low-dose helical CT scan (~ 16 mrem) was acquired for attenuation correction of PET emission data. Following the CT scan, 5 mCi (185 MBq) of [^{18}F]CBD-2115 was injected i.v. as a slow bolus (~ 20 s) followed immediately by a saline flush (~ 10 mL). PET emission data were collected over a period of 90 min in a dynamic series of 27 frames of increasing length (20–600 s). Venous blood samples (~ 3 mL) were collected at five time points after injection (2', 10', 30', 45', and 90') and analyzed by radio-HPLC to characterize the radiolabeled metabolites of [^{18}F]CBD-2115 and determine the time-varying fraction of unmetabolized [^{18}F]CBD-2115. PET emission data were reconstructed using filtered backprojection with Fourier rebinning, and standard data corrections were applied, including those accounting for

physical decay of the radionuclide, photon attenuation, scatter, electronics dead-time, and the quantitative calibration of arbitrary image units (cps/voxel) to absolute units of radioactivity concentration (Bq/mL). A time–activity curve expressed in units of SUV was determined by sampling of the calibrated dynamic image data set using a whole brain region-of-interest defined using PMOD software (v4.0, PMOD Technologies, Zurich, Switzerland).

■ ASSOCIATED CONTENT

SI Supporting Information

The Supporting Information is available free of charge at <https://pubs.acs.org/doi/10.1021/acschemneuro.0c00801>.

Table containing complete results from off target selectivity screening of CBD-2115; table of plasma protein binding and efflux ratios; radiometabolite analysis (PDF)

■ AUTHOR INFORMATION

Corresponding Authors

Samuel Svensson – CBD Solutions, Center for Molecular Medicine, Karolinska Hospital, SE-17176 Stockholm, Sweden; Department of Physics, Chemistry and Biology, Linköping University, SE-58183 Linköping, Sweden; Email: samuel.svensson@cbdsolutions.se

Chester A. Mathis – Department of Radiology, University of Pittsburgh, Pittsburgh, Pennsylvania 15213, United States; Email: mathisca@upmc.edu

Neil Vasdev – Azrieli Centre for Neuro-Radiochemistry, Brain Health Imaging Centre, Centre for Addiction and Mental Health, Toronto, ON MST 1R8, Canada; Department of Psychiatry/Institute of Medical Science, University of Toronto, Toronto, ON MST 1R8, Canada; orcid.org/0000-0002-2087-5125; Email: neil.vasdev@utoronto.ca

Authors

Anton Lindberg – Azrieli Centre for Neuro-Radiochemistry, Brain Health Imaging Centre, Centre for Addiction and Mental Health, Toronto, ON MST 1R8, Canada

Ashley C. Knight – Azrieli Centre for Neuro-Radiochemistry, Brain Health Imaging Centre, Centre for Addiction and Mental Health, Toronto, ON MST 1R8, Canada; Department of Psychiatry/Institute of Medical Science, University of Toronto, Toronto, ON MST 1R8, Canada; orcid.org/0000-0003-2225-360X

Daniel Sohn – CBD Solutions, Center for Molecular Medicine, Karolinska Hospital, SE-17176 Stockholm, Sweden; Novandi Chemistry AB, SE-15136 Södertälje, Sweden

Laszlo Rakos – CBD Solutions, Center for Molecular Medicine, Karolinska Hospital, SE-17176 Stockholm, Sweden; Novandi Chemistry AB, SE-15136 Södertälje, Sweden

Junchao Tong – Azrieli Centre for Neuro-Radiochemistry, Brain Health Imaging Centre, Centre for Addiction and Mental Health, Toronto, ON MST 1R8, Canada

April Radelet – Department of Radiology, University of Pittsburgh, Pittsburgh, Pennsylvania 15213, United States

N. Scott Mason – Department of Radiology, University of Pittsburgh, Pittsburgh, Pennsylvania 15213, United States; orcid.org/0000-0001-7739-3285

Jeffrey S. Stehouwer – Department of Radiology, University of Pittsburgh, Pittsburgh, Pennsylvania 15213, United States

Brian J. Lopresti – Department of Radiology, University of Pittsburgh, Pittsburgh, Pennsylvania 15213, United States

William E. Klunk – Department of Psychiatry, University of Pittsburgh, Pittsburgh, Pennsylvania 15213, United States

Johan Sandell – Novandi Chemistry AB, SE-15136 Södertälje, Sweden

Alexander Sandberg – Department of Physics, Chemistry and Biology, Linköping University, SE-58183 Linköping, Sweden

Per Hammarström – Department of Physics, Chemistry and Biology, Linköping University, SE-58183 Linköping, Sweden

Complete contact information is available at:

<https://pubs.acs.org/10.1021/acscemneuro.0c00801>

Author Contributions

A.L., A.C.K., D.S., L.R., J.T., A.R., N.S.M., J.S.S., B.J.L., J.S., A.S., and P.H. performed research; A.L., A.C.K., J.T., N.S.M., J.S.S., B.J.L., W.E.K., S.S., C.A.M., and N.V. analyzed the data; A.L., C.A.M., and N.V. wrote the paper.

Notes

The authors declare no competing financial interest.

ACKNOWLEDGMENTS

N.V. thanks the National Institute on Ageing of the NIH (R01AG054473 and R01AG052414), the Azrieli Foundation, Canada Foundation for Innovation, Ontario Research Fund, and the Canada Research Chairs Program for support. C.A.M. and N.V. thank the National Institute on Neurological Disorders and Stroke (NINDS) and the NIA (1U19NS110456) as well as the Michael J. Fox Foundation and the Rainwater Charitable Foundation (Tau Consortium) for jointly supporting this research collaboration (Grant 14605). We thank Cerveau Technologies for funding and for allowing the use of [³H]MK-6240, as well as members of the CAMH Brain Health Imaging Centre and the University of Pittsburgh PET Center, with a special thanks to Peter Bloomfield for assistance in rodent PET image reconstruction.

REFERENCES

- (1) Feinstein, H. E., Benbow, S. J., LaPointe, N. E., Patel, N., Ramachandran, S., Do, T. D., Gaylord, M. R., Huskey, N. E., Dressler, N., Korff, M., et al. (2016) Oligomerization of the microtubule-associated protein tau is mediated by its N-terminal sequences: implications for normal and pathological tau action. *J. Neurochem.* 137 (6), 939–954.
- (2) Mukrasch, M. D., Bibow, S., Korukottu, J., Jeganathan, S., Biernat, J., Griesinger, C., Mandelkow, E., and Zweckstetter, M. (2009) Structural Polymorphism of 441-Residue Tau at Single Residue Resolution. *PLoS Biol.* 7 (2), e1000034.
- (3) Novak, P., Cehlar, O., Skrabana, R., and Novak, M. (2018) Tau Conformation as a Target for Disease-Modifying Therapy: The Role of Truncation. *J. Alzheimer's Dis.* 64, S535–S546.
- (4) McKee, A. C., Cantu, R. C., Nowinski, C. J., Hedley-Whyte, E. T., Gavett, B. E., Budson, A. E., Santini, V. E., Lee, H. S., Kubilus, C. A., and Stern, R. A. (2009) Chronic Traumatic Encephalopathy in Athletes: Progressive Tauopathy After Repetitive Head Injury. *J. Neuropathol. Exp. Neurol.* 68 (7), 709–735.
- (5) Delacourte, A., Robitaille, Y., Sergeant, N., Buee, L., Hof, P. R., Watzet, A., Laroche-Cholette, A., Mathieu, J., Chagnon, P., and Gauvreau, D. (1996) Specific pathological Tau protein variants characterize Pick's disease. *J. Neuropathol. Exp. Neurol.* 55 (2), 159–168.
- (6) Albert, M. L., Feldman, R. G., and Willis, A. L. (1974) Subcortical dementia of progressive supranuclear palsy. *J. Neurol. Neurosurg. Psychiatry* 37 (2), 121–130.
- (7) Armstrong, M. J., Litvan, I., Lang, A. E., Bak, T. H., Bhatia, K. P., Borroni, B., Boxer, A. L., Dickson, D. W., Grossman, M., Hallett, M.,

et al. (2013) Criteria for the diagnosis of corticobasal degeneration. *Neurology* 80 (5), 496–503.

(8) Buee, L., and Delacourte, A. (1999) Comparative biochemistry of tau in progressive supranuclear palsy, corticobasal degeneration, FTDP-17 and Pick's disease. *Brain Pathol.* 9 (4), 681–693.

(9) Rabinovici, G. D., Furst, A. J., O'Neil, J. P., Racine, C. A., Mormino, E. C., Baker, S. L., Chetty, S., Patel, P., Pagliaro, T. A., Klunk, W. E., et al. (2007) C-11-PIB PET imaging in Alzheimer disease and frontotemporal lobar degeneration. *Neurology* 68 (15), 1205–1212.

(10) Villemagne, V. L., Ong, K., Mulligan, R. S., Holl, G., Pejoska, S., Jones, G., O'Keefe, G., Ackerman, U., Tochon-Danguy, H., Chan, J. G., et al. (2011) Amyloid Imaging with F-18-Florbetaben in Alzheimer Disease and Other Dementias. *J. Nucl. Med.* 52 (8), 1210–1217.

(11) Okamura, N., and Yanai, K. (2010) Florbetapir (F-18), a PET imaging agent that binds to amyloid plaques for the potential detection of Alzheimer's disease. *IDrugs* 13 (12), 890–899.

(12) Nelissen, N., Van Laere, K., Thurfell, L., Owenius, R., Vandenbulcke, M., Koole, M., Bormans, G., Brooks, D. J., and Vandenbergh, R. (2009) Phase 1 Study of the Pittsburgh Compound B Derivative F-18-Flutemetamol in Healthy Volunteers and Patients with Probable Alzheimer Disease. *J. Nucl. Med.* 50 (8), 1251–1259.

(13) Leuzy, A., Chiotis, K., Lemoine, L., Gillberg, P. G., Almkvist, O., Rodriguez-Vieitez, E., and Nordberg, A. (2019) Tau PET imaging in neurodegenerative tauopathies—still a challenge. *Mol. Psychiatry* 24 (8), 1112–1134.

(14) Beyer, L., Nitschmann, A., Barthel, H., van Eimeren, T., Unterrainer, M., Sauerbeck, J., Marek, K., Song, M. M., Palleis, C., and Respondek, G. (2020) Early-phase F-18 PI-2620 tau-PET imaging as a surrogate marker of neuronal injury. *Eur. J. Nucl. Med. Mol. Imaging* 47, 2911.

(15) Declercq, L., Celen, S., Lecina, J., Ahamed, M., Tousseyn, T., Moechars, D., Alcazar, J., Ariza, M., Fierens, K., and Bottelbergs, A. (2016) Comparison of New Tau PET-Tracer Candidates With F-18 T808 and F-18 T807. *Mol. Imaging* 15, 153601211562492.

(16) Weng, C. C., Hsiao, I. T., Yang, Q. F., Yao, C. H., Tai, C. Y., Wu, M. F., Yen, T. C., Jang, M. K., and Lin, K. J. (2020) Characterization of F-18-PM-PBB3 (F-18-APN-1607) Uptake in the rTg4510 Mouse Model of Tauopathy. *Molecules* 25 (7), 1750.

(17) Jack, C. R., Bernstein, M. A., Fox, N. C., Thompson, P., Alexander, G., Harvey, D., Borowski, B., Britson, P. J., Whitwell, J. L., Ward, C., et al. (2008) The Alzheimer's Disease Neuroimaging Initiative (ADNI): MRI methods. *J. Magn. Reson. Imaging* 27 (4), 685–691.

(18) Greaves, C. V., and Rohrer, J. D. (2019) An update on genetic frontotemporal dementia. *J. Neurol.* 266 (8), 2075–2086.

(19) Luong, D., Voltarelli, L., Heuer, H., Kornak, J., Domoto-Reilly, K., Dickerson, B., Litvan, I., Tartaglia, M. C., Miller, B., and Boxer, A. (2016) Measuring clinical and cognitive decline in CBD and PSP for multicenter clinical trials - the 4-repeat tauopathy neuroimaging initiative (4RTNI). *J. Neurochem.* 138, 371–371.

(20) Rosler, T. W., Marvian, A. T., Brendel, M., Nykanen, N. P., Hollerhage, M., Schwarz, S. C., Hopfner, F., Koeglsperger, T., Respondek, G., and Schweyer, K. (2019) Four-repeat tauopathies. *Prog. Neurobiol.* 180, 101644.

(21) Kroth, H., Oden, F., Molette, J., Schieferstein, H., Capotosti, F., Mueller, A., Berndt, M., Schmitt-Willich, H., Darmency, V., Gabellieri, E., et al. (2019) Discovery and preclinical characterization of F-18 PI-2620, a next-generation tau PET tracer for the assessment of tau pathology in Alzheimer's disease and other tauopathies. *Eur. J. Nucl. Med. Mol. Imaging* 46 (10), 2178–2189.

(22) Li, L., Lu, J. Y., Li, M., Sun, Y. M., Li, X. M., Guan, Y. H., Wang, J., and Zuo, C. T. (2020) Binding Characteristics of the New-Generation Tau PET Tracer F-18 -APN-1607 in Progressive Supranuclear Palsy. *J. Nucl. Med.* 61 (S1), 461.

(23) Sohn, D. (2019) Selective ligands for tau aggregates. Int. Patent WO 2019/1917502 A1.

(24) Pike, V. W. (2016) Considerations in the Development of Reversibly Binding PET Radioligands for Brain Imaging. *Curr. Med. Chem.* 23 (18), 1818–1869.

(25) Wager, T. T., Hou, X. J., Verhoest, P. R., and Villalobos, A. (2010) Moving beyond Rules: The Development of a Central Nervous System Multiparameter Optimization (CNS MPO) Approach To Enable Alignment of Druglike Properties. *ACS Chem. Neurosci.* 1 (6), 435–449.

(26) Biernat, J., Mandelkow, E. M., Schroter, C., Lichtenbergkraag, B., Steiner, B., Berling, B., Meyer, H., Mercken, M., Vandermeeren, A., Goedert, M., et al. (1992) The switch of tau-protein to an alzheimer-like state includes the phosphorylation of 2 serine proline motifs upstream of the microtubule binding region. *EMBO J.* 11 (4), 1593–1597.

(27) Wilson, A. A., Jin, L., Garcia, A., DaSilva, J. N., and Houle, S. (2001) An admonition when measuring the lipophilicity of radiotracers using counting techniques. *Appl. Radiat. Isot.* 54 (2), 203–208.

(28) Klunk, W. E., Wang, Y. M., Huang, G. F., Debnath, M. L., Holt, D. P., and Mathis, C. A. (2001) Uncharged thioflavin-T derivatives bind to amyloid-beta protein with high affinity and readily enter the brain. *Life Sci.* 69 (13), 1471–1484.

(29) Dorr, A. E., Lerch, J. P., Spring, S., Kabani, N., and Henkelman, R. M. (2008) High resolution three-dimensional brain atlas using an average magnetic resonance image of 40 adult C57Bl/6J mice. *NeuroImage* 42 (1), 60–69.

(30) Schwarz, A. J., Danckaert, A., Reese, T., Gozzi, A., Paxinos, G., Watson, C., Merlo-Pich, E. V., and Bifone, A. (2006) A stereotaxic MRI template set for the rat brain with tissue class distribution maps and co-registered anatomical atlas: Application to pharmacological MRI. *NeuroImage* 32 (2), 538–550.